Characterisation of a BC501A compact neutron spectrometer for fusion research

G. Tardini[1]‡, F. Gagnon-Moisan[2,3], A. Zimbal[2]

[1] **MPI für Plasmaphysik, Euratom Association, Boltzmannstr. 2, 85748 Garching, Germany**

[2] **Physikalisch-Technische Bundesanstalt, Bundesallee 100, 38116 Braunschweig, Germany**

[3] **Paul Scherrer Institut, 5232 Villigen PSI, Switzerland**

Abstract. The Compact Neutron Spectrometer used at the ASDEX Upgrade tokamak is characterised to obtain its response matrix. This paper describes the characterisation procedure and the derived response matrix, based on a campaign at the PTB ion accelerator facility (PIAF) and on the subsequent time-of-flight (TOF) analysis of neutrons from a field with a broad energy distribution. The response of mono-energetic neutrons generated at the PIAF is used as reference for the TOF analysis. The detector's response functions for spectrum deconvolution is obtained by Gaussian broadening of simulated responses to fit the experimental ones, using a maximum-entropy ansatz. In this way, the response functions are smooth enough to ensure a reliable unfolding of pulse height spectra into neutron emission spectra,

‡ Corresponding author: git@ipp.mpg.de

which provide information on the fast ion velocity distribution in neutral beam heated tokamak plasmas.

Keywords: neutron; spectrometer; tokamak; nuclear fusion

1. Introduction

In tokamak research, measurements of the fast ion distribution are gaining growing attention, as the confinement of supra-thermal ions plays a key role in terms of fusion performance, potential damage of the plasma facing components and interplay with magneto-hydrodynamic (MHD) instabilities such as Alfven eigenmodes [1][2], neoclassical tearing modes [3] and sawteeth [4], all representing serious concerns for next-step tokamaks like ITER.

Neutron emission spectra (NES) provide energy-resolved information on the fast ion distribution, whenever beam-target reactions dominate the neutron production, which is the case in Neutral Beam Injection (NBI) discharges, in the ASDEX Upgrade tokamak [5] as well as in most NBI heated devices. Diagnostic systems to measure energy resolved NES are usually expensive and require a large dedicated volume [6]. These limitations are overcome by Compact Neutron Spectrometers (CNS). However, CNS cannot determine the neutron energy for each event occurring in the detector, but it rather allows to measure the deposited energy from recoil protons, for all possible scattering angles. The histogram of the occurrence of such deposited energies with a given energy binning is the so-called Pulse Height Spectrum (PHS). Therefore, the determination of the energy distribution of the incoming neutrons requires a deconvolution of the measured PHS, using the detector's characteristic response functions. To obtain useful NES, unfolding uncertainties and artifacts have to be minimised. Therefore, the detector's response matrix has to be determined with high accuracy and it requires

a sufficient degree of smoothness.

At ASDEX Upgrade a CNS is available, based on the liquid scintillator BC501A [7][8]. The detector was brought to the facility at the Physikalisch-Technische Bundesanstalt (PTB) to collect measurements of its response to neutrons with known energy, either mono-energetic D-d neutrons from the accelerator or neutrons selected from a pulsed neutron field with broad energy distribution via their TOF.

The details of the characterisation procedure and the determination of the detector response matrix are the subject of this paper. The facility and the setup of the experimental campaign are described in Section 2. The evaluation of the resulting experimental response matrix is presented in Section 3, including some analysis details. Finally, in Section 4 the fitting procedure of the simulated responses to the experimental ones is explained and applied, before conclusions are drawn in Section 5.

2. Facility and setup for the experimental characterisation campaign

The experimental campaign for the characterisation of the CNS was performed at the PTB Ion Accelerator Facility, particularly suited for these measurements [9]. The facility consists of a room for the cyclotron and the target and of an experimental hall for the detector. Well collimated line-of-sights provide a convenient location for the detector. The PTB cyclotron accelerates a deuterium beam onto a gas deuterium target, yielding mono-energetic D-d neutrons at energies of 8, 10, 12 and 14 MeV at the fixed observation angle. Moreover, hitting a 3 mm ^{9}Be layer with accelerated protons one can generate a

broad neutron energy spectrum, the so called "white field".

The detector was placed at (20.12 ± 0.01) m, the highest available distance, in order to achieve the longest possible time-of-flight (TOF) of neutrons from the source to the detector. In this way, the neutron energies are better separated. The repetition rate was 500 kHz, a trade-off between high statistics and TOF resolution. Additional measurements of γ photons from ^{207}Bi decays were collected for calibration purposes. The TOF evaluation needs an absolute time reference. The TOF scale is derived using a reference signal from the cyclotron and the signals from target-generated gamma events which have a known TOF to the position of the detector.

3. Evaluation of the experimental response matrix

3.1. Pulse shape discrimination

For the preliminary analysis, a Digital Pulse Shape Discrimination (DPSD) software [7] is used, written in C++ within the ROOT framework [11], particularly suited for the analysis of large data volumes, for a GUI-based user control and for graphic output. The DPSD code allows to discard gamma events from the following evaluation, taking advantage of the shorter scintillation time of gamma pulses for a given pulse light output [7]. The pulse characteristics, output of the DPSD analysis, are stored in database-structured, compressed ROOT files. Figure 1 shows the degree of separation between neutron and gamma pulses, the 2-sloped red line being the flagging criterion.

Since pulses are digitalised via a digital acquisition system, the pulse shape is defined

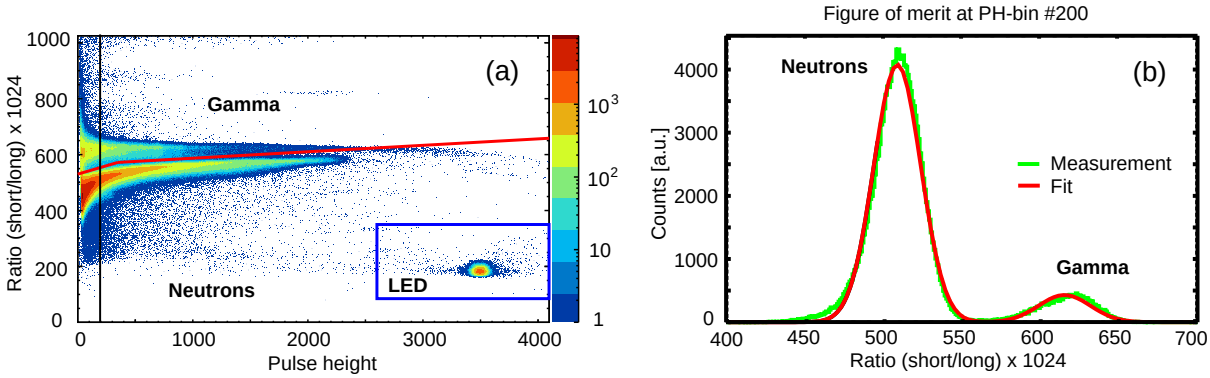

Figure 1. (a) Long/Short gate ratio for the acquisitions in the ^{9}Be+p field, versus total gate. The blue rectangle marks the region of LED pulses for off-line gain correction. The 2-sloped red line is used for γ-n discrimination. (b) Figure of merit of the γ-n separation at PH channel 200, marked as vertical black line in (a). PH-bin #200 corresponds to $E_{light} \sim 1$ MeVee.

as the ratio between the pulse integral in a short and a long time interval after the pulse peak [7], whereas the Pulse Height (PH) is the total pulse integral. A good separation is obtained using 3 samples for the short interval and 14 for the long one, corresponding to 15 and 70 ns, respectively. The figure of merit $\Delta_{n-\gamma}$ of the separation is defined here as $\Delta_{n-\gamma} = \frac{x_{peak1}-x_{peak2}}{FWHM1+FWHM2}$ where x_{peak} represents the location of the maximum of the respective gaussian fit. The values of $\Delta_{n-\gamma}$ for different PH channels are summarised in table 1. An example for PH-bin #200 is shown in Fig. 1 (b).

LED light pulses are triggered, providing a reference for the photo-multiplier gain, which is known to be count-rate-dependent. This allows an a posteriori correction for the pulse height, however such a correction factor in this campaign is almost constant in time, because the count rate is stable during the experiment. Therefore, the LED repetition rate was set to 2 Hz only, compared to the usual 1 kHz during plasma experiments.

E_{light} [MeVee]	$\Delta_{n-\gamma}$
0.5	1.38
1	1.59
1.5	1.63
2	1.58
2.5	1.54
3	1.49
3.5	1.41
4.	1.31
4.5	1.21
5.	1.13

Table 1. $\Delta_{n-\gamma}$ as a function of the pulse height.

LED events are well separated in the pulse height-pulse shape diagram, as shown in Fig. 1 (a).

For each neutron event the TOF is evaluated using the next cyclotron pulse as reference. The zero point of the TOF scale for neutrons is provided by photons, who travel at known speed. Since we use a later time point as reference, in TOF spectra the X-axis is actually $t_{ref} - TOF$, so that faster neutrons are associated with higher times in the plot (e.g. Fig. 2). Further details of this method of TOF analysis are illustrated in [10], paragraph 5.1.

3.2. Satellite removal

To produce the white field with neutron energies up to 17 MeV, a proton beam of about 19 MeV hits a ^{9}Be layer. Due to the long flight distance of 20 m, only a fraction of the proton pulses can be used to get a time of flight distribution with no overlap of pulses. Therefore the internal cyclotron frequency had to be reduced from several MHz to 500 kHz. This is done by deflecting certain proton pulses out of the proton beam electrostatically. Some of the protons, however, are not perfectly deflected by the beam pulse selector. As a consequence, the TOF spectrum contains "ghost images". There are called "satellites" and have significantly lower counts, while displaying the same structure as the main TOF-distribution. Since we aim at correct counts in the PH-TOF diagram (Fig. 2), it is not relevant whether a single event is a satellite event or not. A statistical determination of the satellite probability density in each diagram pixel is sufficient. This is done with the Time Of Flight ANAlysis (TOFANA) code [10]. In the TOF spectrum diagram (Fig. 2) the user can define up to 8 TOF intervals for satellite peaks, either interactively or loading an ASCII file. The events in the upper PH region (between the two horizontal red lines in Fig. 2) are then counted and normalised to the number of counts of the main structure in the same region, yielding a probability density factor for each satellite structure. The method is described in detail in Section 5.3 of [10]. The ROOT framework [11] of the TOFANA code allows to select a region by defining the coordinates of a closed broken line, such as the magenta one in Fig. 2. Again, the broken line can be selected either interactively on the graphic canvas or

by a pre-defined input file, containing the coordinates of the knots of the broken line. Using the file input ensures reproducibility, making the analysis more accurate and less time-consuming. The spectrum contained in the selected region represents the main histogram. Since satellites have the same shape and relative distribution as the main peak, we clone the main histogram into n_{sat} histograms, one per satellite structure. Each clone is shifted by the distance between its peak and the peak of the main structure, then multiplied by its probability density factor and eventually subtracted from the main histogram. In this way, we are left with a satellite-free PH-TOF diagram (see Fig. 3),

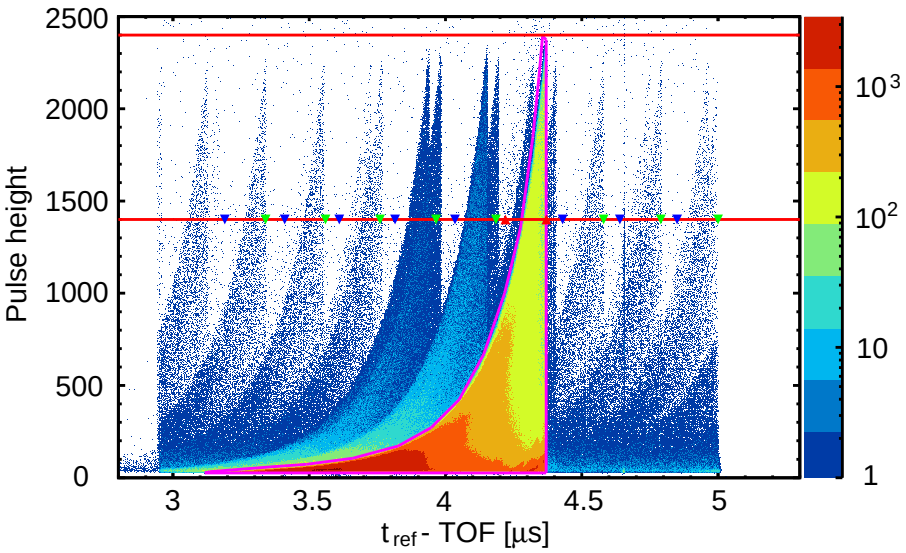

Figure 2. TOF spectrum including satellites. The cut region (magenta broken line) and the satellite evaluation region (horizontal red lines) are highlighted, as well as the TOF-ranges for satellite peaks (blue-green triangles).

which is the basis for further analysis. Overlap between neighbouring satellite structures limits the accuracy of this subtraction procedure. In our campaign, satellites amount to roughly 4 % of the total detected neutron pulses. The experimental response matrix

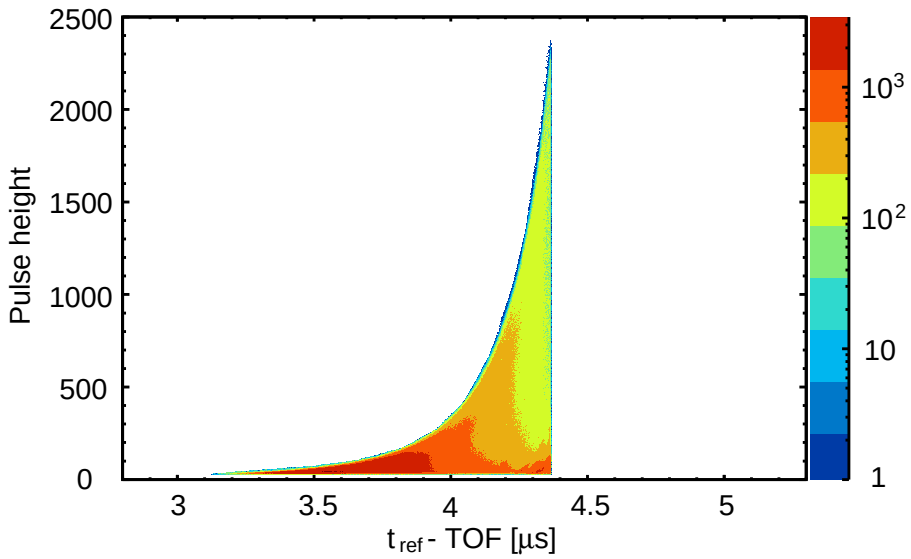

Figure 3. TOF spectrum after satellites have been removed.

can be derived by selecting narrow energy (and hence TOF) intervals and evaluating the PHS. It corresponds to several vertical cuts of the contour plot of Fig. 3. The intervals' widths are chosen to have enough statistics for a smooth PHS without having a too wide energy range in each single interval. A good trade-off is $\Delta E/E = 1$ %, as the energy interval is narrow while the counts are high enough to have low statistical noise, comparable to that of the mono-energetic PHS. This is the energy width used for the selection of the energy intervals in the following. The FWHM of the mono-energetic spectra is $\Delta E/E \approx 0.2$ %, for reference.

3.3. Comparison with mono-energetic neutrons

An important check of our TOF calibration is the comparison with the PHS measured in a mono-energetic neutron field. The PTB cyclotron was setup to obtain D-d neutrons at energies of 8, 10, 12 and 14 MeV. By selecting TOF intervals corresponding to

energies around these values, we can evaluate the accuracy of our TOF estimation. The comparison is shown in Fig. 4. Note that break-up reactions occur for D-D reactions for energies above 6-7 MeV. Such events are filtered out by selecting narrow TOF intervals also for the mono-energetic neutrons. The resulting agreement is excellent, within the uncertainty of the distance measurement.

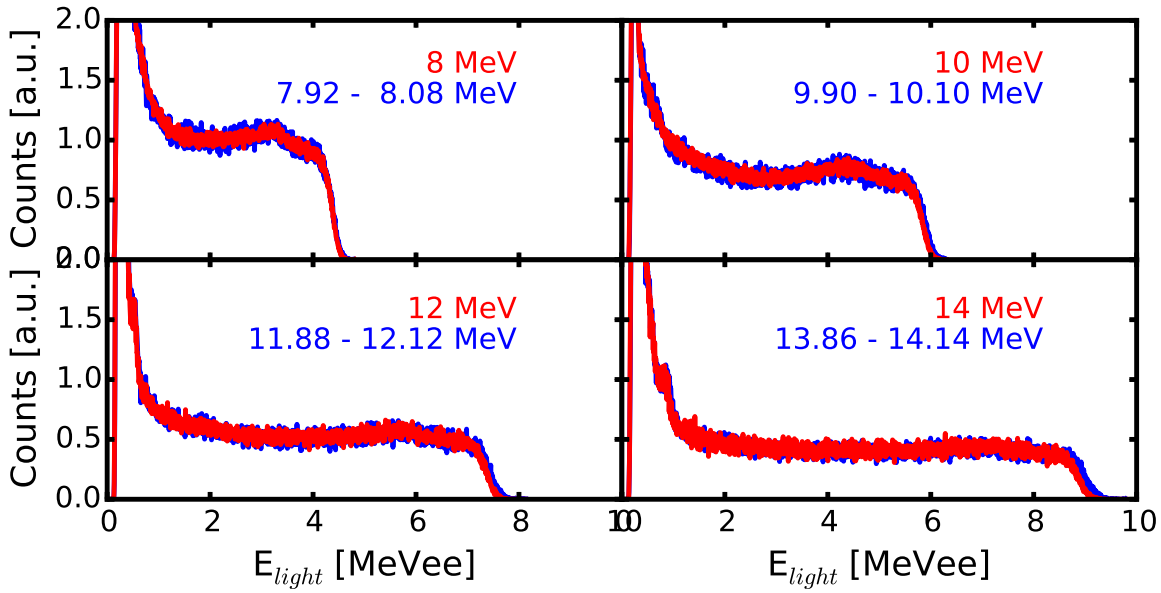

Figure 4. Comparison between PHS from mono-energetic neutrons (red) and selecting TOF intervals (blue) around the nominal values of 8, 10, 12 and 14 MeV.

4. Fitting the simulated response matrix

We select 30 narrow TOF intervals around energy values from 1.5 to 16 MeV and evaluate the experimental response matrix rejecting gamma pulses and satellite events. Simulations with the NRESP code [12] covering the whole energy range are used as starting point of the fitting procedure. An initial estimate for the detector's light output

function is provided by the function determined for a similar BC501A-based CNS. The comparison of the initial simulated responses with the experimental ones is shown in Fig. 5. The gamma spectrum emitted by a ^{207}Bi source is also measured and compared

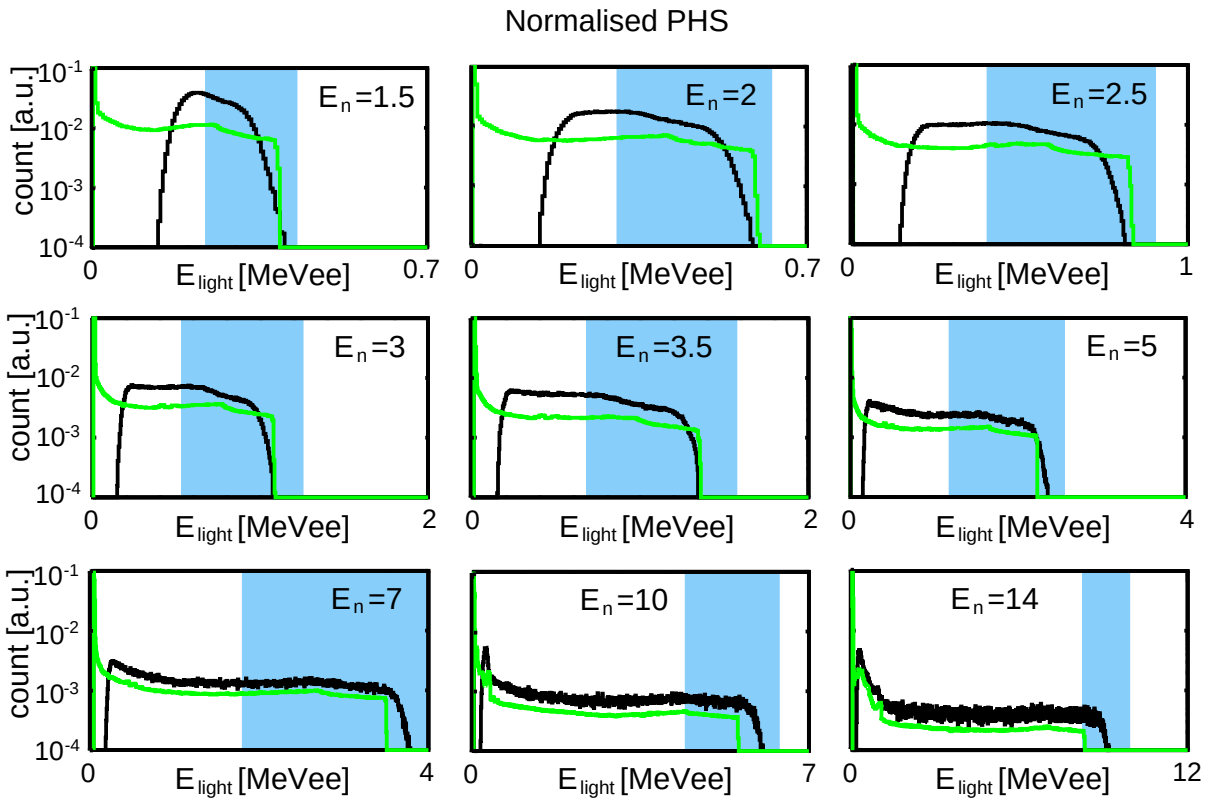

Figure 5. Experimental response functions (black) and initial estimate with NRESP simulations (green), with logarithmic scale for the y-axis. The blue regions mark the intervals considered for optimisation in each PHS. Each subplot has a label for the corresponding neutron energy in MeV.

to simulations done with the PHRESP code [18]. ^{207}Bi has the favourable property of having 3 sharp lines in the MeV range, at 0.569, 1.063 and 1.770 MeV, thus allowing to decouple offset and calibration coefficient of the light output scale.

4.1. Adjustment of the light output function

For each of the 30 considered neutron responses the pulse-height axis (x-axis) is allowed to have a different stretching factor in the fitting procedure, based on maximum-entropy [10]. This method is a generalisation of the χ^2 method, its main advantages are discussed in [19]. A comparison between the maximum-entropy and the χ^2 method, concerning specifically the characterisation of scintillation detectors, is discussed in [20].

Once optimisation is reached, their final values are used to modify the light output function via simple interpolation. In Fig. 6 the initial estimate is compared with the actual CNS light output function. Moreover, additional fitting parameters are

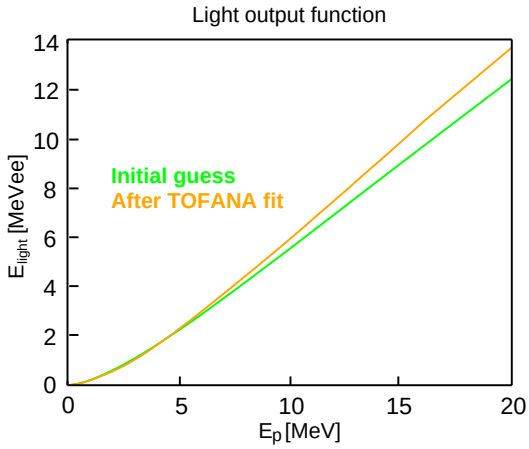

Figure 6. Detector light output function: initial estimate (green) and actual (red) after optimising the fit

the broadening coefficients a, b and c, defined by the relation $dL(L) = 0.01 * \sqrt{a^2L^2 + b^2L + c^2}$ L being the light output function of the recoil-proton in MeVee and dL the local value of the full width half maximum used for the Gaussian convolution. The broadening coefficients a, b, and c and the offset scale-parameter z are common to

all 30 responses, as well as for the fit of the gamma response.

4.2. Broadened response function and energy resolution

The correct light output function is then applied to a new set of NRESP simulations. The simulated PHS are then used for a second (and final) fit of the experimental responses. As expected, the stretching factors for the pulse height scale axis are now unity for all PHS within 0.5 %, which is the confirmation a posteriori that the light output function has been determined correctly to a satisfying degree of accuracy. The optimised Gaussian fit is shown in Fig. 7. The output fitting parameters are a=3.798, b=7.301, c=0.6001, z=-0.02847. The pulse height resolution function dL/L is 10.3% for E_n = 2.5 MeV (approximately the d-d neutron energy) and 4.6% for E_n = 14 MeV, the characteristic neutron energy from D-T fusion reactions. The gamma spectrum of the ^{207}Bi source is also fitted within the same relative entropy maximisation procedure. The accuracy of the fit is shown in Fig. 8. The match is excellent apart from the region between 1 and 1.5 MeV. This is due to the coincident emission at 1064 and 570 MeV by the daughter nucleus ^{207}Pb, which is not always recongnised as double peak due to the simultaneous emission, resulting in superposed PHS. However, the fit is used here only to calibrate the energy axis and to evaluate the instrument energy resolution, therefore only the accuracy of the selected regions matters, both in terms of location and broadening of the falling edges. The Gaussian broadening is then applied to the whole set of simulated neutron response functions, which are then used for the deconvolution

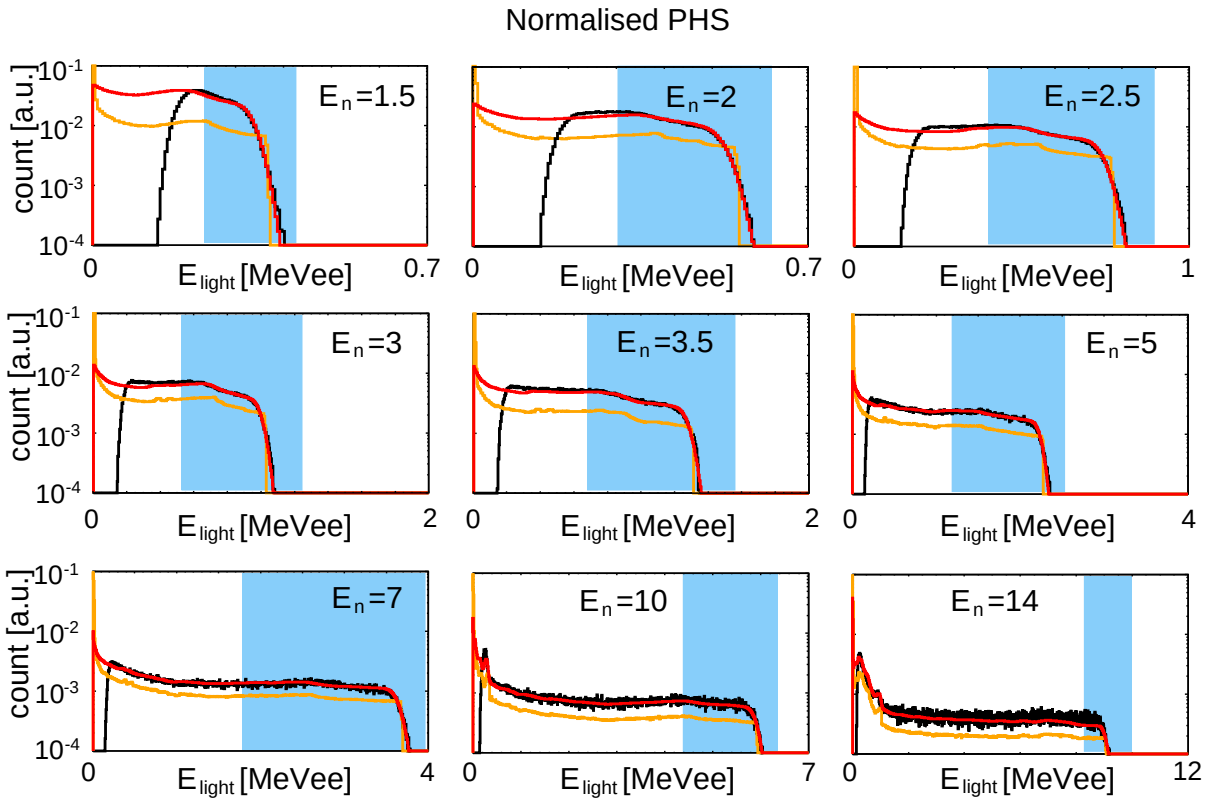

Figure 7. Corrected simulated response functions (orange) and Gaussian broadened responses (red) to fit the measured response functions (black), with logarithmic scale for the y-axis. The blue regions mark the intervals considered for optimisation in each PHS. Each subplot has a label for the corresponding neutron energy in MeV.

of the measured PHS. The Gaussian broadened simulated response PHS, in fact, are smoother than the experimental ones and therefore they are less prone to artifacts and uncertainties in the deconvolution. Moreover, they are automatically normalised to unit fluency, due to the internal normalisation of the NRESP code, which is important for a correct unfolding. However, by re-normalising the experimental responses also an experimental response matrix is determined.

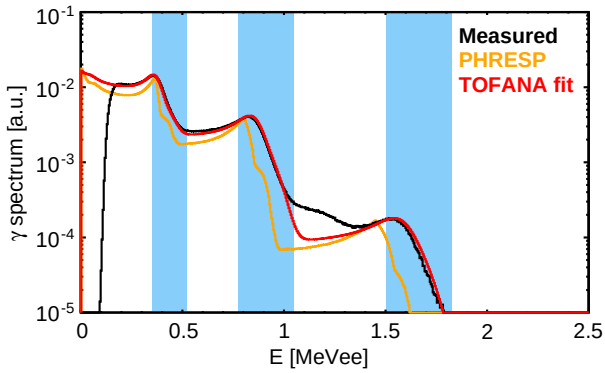

Figure 8. PHRESP-simulated gamma response before (orange) and after Gaussian broadening and x-axis rescaling (red) to match the experimental ones (black), with logarithmic scale for the y-axis. The blue regions mark the intervals considered for optimisation of each peak.

5. Conclusions

The CNS detector employed on the ASDEX Upgrade tokamak, based on a BC501A liquid scintillator, has been fully characterised at the PTB accelerator facility. The separation between neutron and gamma events proves excellent, with values of $\Delta_{n-\gamma} > 1$ over the relevant PH range. Measurements with mono-energetic neutrons are used to validate the TOF analysis of the detector response to a "white neutron field". By choosing $\Delta E/E = 1$ % around the discrete energy values, the agreement with the monoenergetic neutrons is shown to be excellent in terms of the PHS shape and concerning the slope of the falling edge. The bin-location of the falling edge is also in good agreement, within the uncertainties such as the exact distance of the detector from the source.

The TOFANA code used for analysis has been further developed, improving speed,

user-interface and compatibility with the code for digital pulse shape discrimination, also based on C++/ROOT.

As a result, both an experimental and a simulated response matrix are determined, the latter by optimising a Gaussian broadening of NRESP-calculated responses at energies close to those selected for the experimental analysis, with a maximum-entropy ansatz. The pulse height resolution is in good agreement with the one determined previously for a similar detector [10], with $dL/L = 10.3\%$ at $E_n = 2.5$ MeV and $dL/L = 4.6\%$ at $E_n = 14$ MeV.

The simulated and broadened response matrix can be now used for deconvolution of the experimental PHS, providing a useful tool to extract information about the supra-thermal ion population in tokamaks.

[1] C. Z. Cheng *et al.*, Ann. Phys 161 **21** (1985)

[2] Ph. Lauber, Phys. Reports. **533** (2013) 33

[3] R. B. White and M. S. Chance, Phys. Fluids **27** (1984) 2455

[4] B. Geiger *et al.*, Plasma Physics and Controlled Fusion **53** (2011) 065010

[5] G. Tardini *et al.*, Nuclear Fusion **53** (2013) 063027

[6] M. Gatu Johnson *et al.*, Nuclear Instruments and Methods in Physics Research A **591** (2008) 417

[7] G. Tardini *et al.*, Journal of Instrumentation **7** (2012) C03004

[8] L. Giacomelli *et al.*, Review of Scientific Instrument **82** (2011) 123504

[9] R. Nolte *et al.*, Radiat. Prot. Dosim. **110** (2004) 97

[10] F. Gagnon-Moisan *et al.*, Journal of Instrumentation **7** (2012) C02023

[11] Rene Brun and Fons Rademakers, Proceedings AIHENP'96 Workshop, Lausanne, Sep. 1996, Nucl. Inst. & Meth. in Phys. Res. A **389** (1997) 81-86. See also http://root.cern.ch/

[12] G. Dietzke and H. Klein, Physikalisch-Technische Bundesanstalt Report PTB-ND-22, Braunschweig, Germany (1982)

[13] M. Reginatto, A. Zimbal, Rev. Sci. Instruments **79** (2008) 023505

[14] R. Bilato *et al.*, Nuclear Fusion **51** (2011) 103034

[15] A. Pankin, D. McCune, R. Andre *et al*, Comp. Phys. Comm. **159**, No. 3 (2004) 157

[16] B. H. Park *et al.*, Paper JP8.00122, Bull. Am. Phys. Soc. 54, (2012)

[17] M. Nocente *et al.*, Nuclear Fusion **51** (2011) 063011

[18] D. Schmidt and H. Klein, Physikalisch-Technische Bundesanstalt Report PTB-N-35, Braunschweig, Germany (1998).

[19] E.T. Jaynes, "Probability Theory: The Logic of Science", Cambridge U.P., Cambridge (2003), Chapter 9

[20] F. Gagnon-Moisan, A. Zimbal and M. Reginatto, "New developments for the determination of the response function for a BC501A compact neutron spectrometer for fusion diagnostics", Proc. of Advancements in Nuclear Instrumentation, Measurement Methods and their Applications, June, 6-9, 2011 ICC, Ghent, Belgium